Acid/Base, Copper Binding, and Cu 2+ /H + Exchange Properties of Goethite, an Experimental and Modeling Study

ARTICLE *in* ENVIRONMENTAL SCIENCE AND TECHNOLOGY · SEPTEMBER 1998

Impact Factor: 5.33 · DOI: 10.1021/es9709942

2 AUTHORS, INCLUDING:

James Leckie
Stanford University
47 PUBLICATIONS **2,162** CITATIONS

SEE PROFILE

Environ. Sci. Technol. **1998**, *32,* 2519−2530

Acid/Base, Copper Binding, and Cu^{2+}/H^{+} Exchange Properties of Goethite, an Experimental and Modeling Study

A. P. ROBERTSON* AND J. O. LECKIE

Environmental Engineering and Science, Department of Civil and Environmental Engineering, Stanford University, Stanford, California 94305

For aquatic systems, the movement, fate, and impact of trace metals strongly depend on the metal's tendency to partition to surfaces. An experimental and modeling study of proton and copper(II) sorption and Cu^{2+}/H^{+}exchange to goethite (α-FeOOH), an important oxide mineral, was conducted. Copper partitioning data covered three pHs, two ionic strengths, three orders of magnitude in copper surface coverage, and six orders of magnitude in solution copper(II) activity. Three surface complexation models [diffuse layer model (DLM), triple-layer model (TLM), and modified triple-layer model (Mod TL)] successfully replicated copper partitioning when at least two classes of copper binding sites, differing significantly in copper binding affinity, were included in the analysis. The (combination of) surface complex(es) that fit the data well depends on the model employed. Fits to the copper partitioning data do not permit selection of a "best" model/complex(es) combination. However, only the TLM and Mod TL reasonably replicate the proton partitioning (acid/base) properties of the goethite.

Introduction

The transport, speciation, availability, and fate of trace metals such as copper, cadmium, selenium, and uranium are important environmental concerns primarily because these metals can be toxic to living organisms. Much metal cycling occurs naturally; however, man's activities, both directly and indirectly, mobilize metals (*1, 2*). Emissions from cars, power plants, and smelting operations put metals in the air; their deposition increases loadings to soil and aquatic systems. Mining and ore processing operations often expose metal-bearing minerals to conditions that facilitate their dissolution, increasing their bioavailability and the potential for transport. Nuclear power and weapons production create and concentrate considerable quantities of metal radionuclides. Wastes from manufacturing processes and corrosion or leaching from metal-containing products may mobilize significant amounts of metal. Irrigation may release, to the water column, metals resident in soils.

In aqueous systems, a metal's toxicity depends on its speciation; bioavailability and toxicity often appear to be proportional to the activity of the free metal ion (*3, 4*). Behavior is complicated because metals may partition to and from mineral surfaces and macromolecules, precipitate and dissolve, form complexes with solution species, and change oxidation state. The extent and rate of these processes depend, often in complex ways, upon solution conditions (including pH, pE, ionic strength, and chemical composition) and the composition of soil, sediment, or colloidal phases. The partitioning of metals to mineral, soil, and colloidal particles strongly affects their transport and availability. The ability to understand and describe this partitioning, its mechanisms and controls, is important if we are to accurately assess the environmental impacts of metals.

Though often a small fraction of the total mass, oxide minerals are important components of soil, rock, and sediment systems. They often exist as colloids or coatings, representing a significant fraction of the surface area available for interaction with the solution and its constituents (*5*).

Our work with goethite (α-FeOOH), a common iron oxide (*6*), was part of a study that looked at how mineral−organic polymer (goethite−humic acid) interactions affect metal (copper) behavior (*7, 8*). Such effects may be important in the many aqueous and soil systems where minerals and organic polymers intimately associate (*9*−*12*).

Surface complexation models (SCMs) are used to replicate, predict, and understand the acid−base and metal binding properties of oxide surfaces (*13*−*16*). Several model constructs exist. They differ in how the interfacial region is structured, whether multiple crystal faces are assumed, whether all sites are identical, and whether, over the range of natural pHs, sites can assume two or three protonation states (*13*−*15, 17*−*23*). We fit the goethite data with three SCMs that vary in their representation of the interfacial region. The results shed light on what can be inferred from modeling and how assumptions about interfacial region structure influence model behavior.

Materials and Methods

Unless otherwise noted, all chemicals used were reagent grade. Experiments were conducted at 25 °C on 100 mL of 10.0 g/L goethite solutions (sodium perchlorate electrolyte), using a computer-controlled titration system that measured and recorded the response of pH- and copper(II)-sensing electrodes and controlled and recorded the addition of acid, base, and copper titrant (*24*). The Davies equation was used to convert between concentrations and activities (*3*).

Goethite Preparation. Goethite was synthesized using essentially the method of Atkinson et al. (*24, 25*). During synthesis exposure of goethite to CO_2 was minimized by using carbonate-free sodium hydroxide and boiled Milli Q water and by purging the container with argon. After dialysis, goethite was stored as a slurry (∼100 g/L) at 4 °C in a polypropylene container. BET and XRD analyses of freeze-dried samples showed the mineral to be goethite with a surface area of 49 m^2/g. Primary stock solutions were made from the slurry by dilution with CO_2-free Milli Q water and electrolyte solutions and calibrated acid, with a final pH of 4.3−5; $I = 1-2 \times 10^{-3}$ M.

Titrants. Calibrated acid ($HClO_4$), carbonate-free base (NaOH), and copper [$Cu(ClO_4)_2$] solutions were used as titrants. Normalities of the acid and base solutions were determined by titration against sodium carbonate (Na_2CO_3) and potassium hydrogen phthalate ($KOOCC_6H_4COOH$) solutions, respectively (*26*). A standard copper solution was prepared by dissolving Supra Pur (99.999%) cupric oxide

* To whom correspondence should be addressed. Telephone: (650)723-0315; fax: (650)725-3164; e-mail: sandrob@alumni.stanford.org.

S0013-936X(97)00994-2 CCC: $15.00
Published on Web 07/25/1998

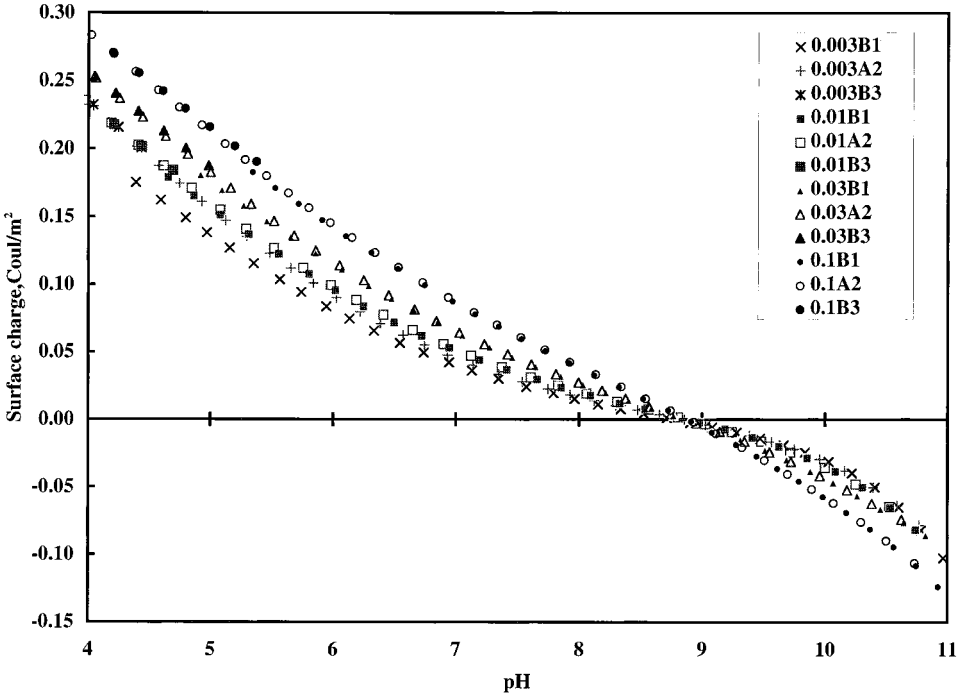

FIGURE 1. Surface charge vs pH for three-legged (base then acid then base) goethite acid−base titrations in sodium perchlorate electrolyte. Initial ionic strengths ranged from 0.003 to 0.1 N: 0.003B1, initial *I* = 0.003 N; B, base leg; and 1, first leg.

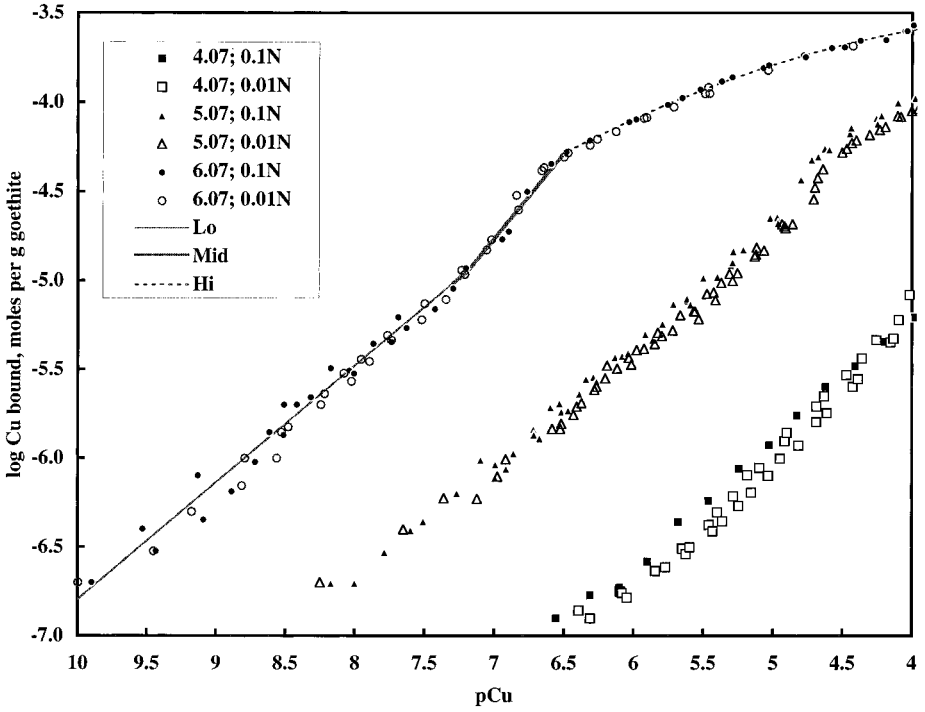

FIGURE 2. Copper binding by goethite at pH 4.07, 5.07 and 6.07 and with ionic strengths of 0.01 and 0.1 N. Solid symbols represent 0.1 N data and open symbols 0.01 N. All data except that for pH 4.07 and 0.1 N include replicate experiments. Lines are regressions of pH 6.07 and 0.1 N results, representing curve regions described in text.

(CuO) in concentrated ultrapure perchloric acid. After dissolution, the supernatant was diluted to give a nominal copper molarity of 0.1 M (pH ~4.6). This solution was standardized with EDTA (*26*). Calibration precisions were ~0.3−0.5%.

Electrode Calibrations. For potentiometric titrations the glass electrode−reference couple was calibrated in two ways: (1) pH buffers (pH 4.00, 7.00, and 10.00) and (2) titration of 100 mL $NaClO_4$ solutions ($I_{calib\ soln} = I_{exptl\ soln}$) with $HClO_4$ and NaOH titrants. Linear regressions of the data provided slopes and intercepts. The two methods generally produced essentially identical, near-Nernstian slopes. Intercepts, calculated from the electrolyte titration data, were generally 2−5 mV higher (average of 4.0 mV) than buffer intercepts. Thus, acid−base calibration curves implied pHs that on average were 0.07 unit higher than buffer data. Determination of goethite surface charge requires knowledge of the solution concentration of H^+ and OH^-. Method 2 directly reflects these concentrations and was used for pH determination.

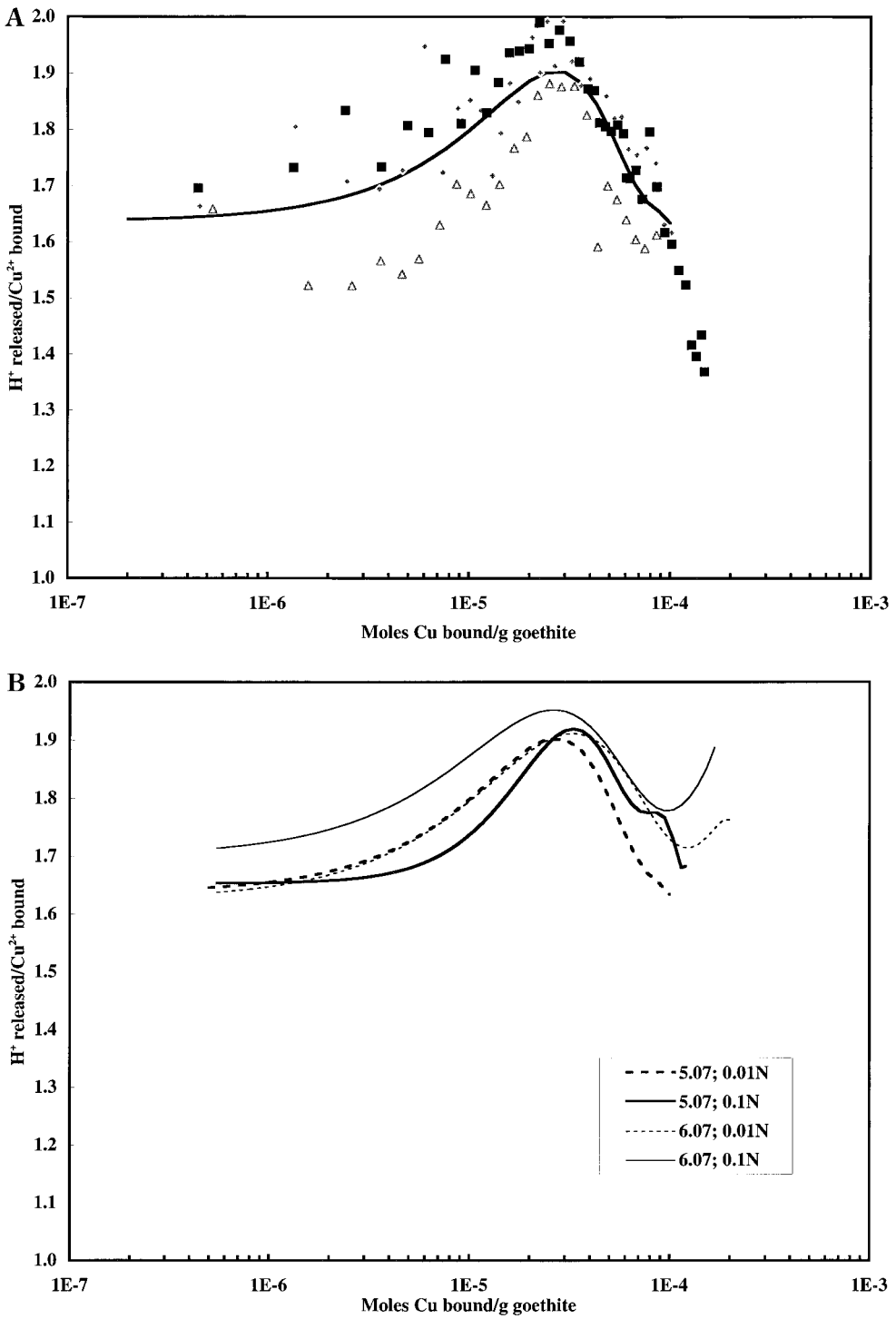

FIGURE 3. Goethite incremental proton release data. (A) Varying symbols represent replicate experiments at pH 5.07 and 0.01 N. The line is a polynomial regression of all data. (B) Polynomial regressions of data at pH 5.07 or 6.07 and 0.01 or 0.1 N.

The pH-statted Cu binding and proton release experiments required calibration of both the glass−reference couple and the Cu ISE−reference couple. Buffers (pH 4.00 and 7.00) were used for the former and titrations of 100 mL $NaClO_4$ solutions ($I_{calib\ soln.} = I_{exptl\ soln}$) with $Cu(ClO_4)_2$ (1.00×10^{-6} to 1.00×10^{-3} M Cu) for the latter. To be consistent with the pH convention used for potentiometric titrations, the buffer-calculated pH 4.00, 5.00, and 6.00 pH-statted experiments were considered to have been conducted at pH 4.07, 5.07, and 6.07, respectively. Cu ISE response was typically linear and near-Nernstian. In simple electrolyte solutions, copper ISEs generally provide a linear response down to $\sim 10^{-6}$ M free copper. With sufficient total copper and a copper complexant, electrode response can remain linear to much lower free copper activity (pCu) (*27*, *28*). Our titrations of solutions containing NTA confirmed the linear ISE response to pCus of ~11 (*24*).

Titrations typically took ~1−2 days to complete, so electrode stability was important. Tests of electrode response in pH buffer solutions (glass−reference couple) and electrolyte solutions containing copper (glass−Cu ISE−reference) showed that the electrodes drifted 2.0 mV or less over a 24 h period.

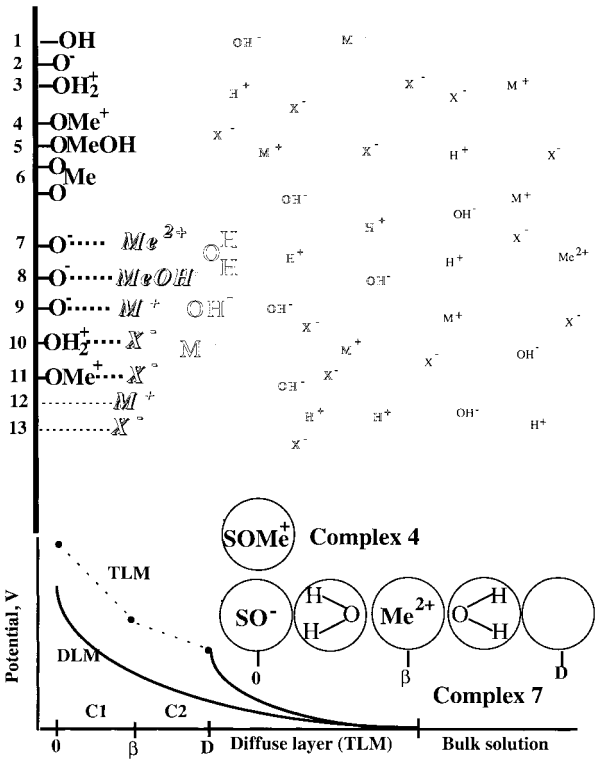

FIGURE 4. Model representation of the oxide surface.

Experimental Details

Goethite solutions were equilibrated for at least 2 days at room temperature and overnight at 25 °C, under argon, before beginning titrations. Solutions for the copper binding and proton exchange experiments were maintained close to the desired pH during this equilibration.

Potentiometric Titrations. Three-legged (base then acid then base) titrations were conducted. Initial pHs were between 4.5 and 5.5, and the titrations were conducted over the pH range of 4−11. Equilibrium was assumed when linear regressions on the periodic pH emf readings taken over a 5 min period gave an emf slope and standard deviation that were sufficiently small, generally less than 0.005 mV/min and 0.04 mV, respectively.

pH-Statted Copper Titrations. Copper (2×10^{-7} mol) was added to the goethite solution just before beginning the overnight, 25° C, argon purge. During titrations, acid or base was added, as necessary, to maintain the desired pH (±0.5 mV). When the Cu ISE emf drift dropped below 0.005 mV/min, equilibrium was assumed and additional copper titrant added. Titrations were continued until the solution copper activity was greater than 1×10^{-4} M.

Proton Release Experiments. Except for the fact that no copper was added before the overnight, 25° C, argon purge, the solution preparation was identical to that for the copper binding experiments. After electrode calibration, the pH of the goethite solution was brought to within 0.1 mV (0.002 pH) of the desired value. Copper (1.0×10^{-6} mol) was added, the ISE placed in the solution, and base added to return the pH to the set point (±0.1 mV). After 7−15 min, the pH and Cu ISE emfs and copper, base, and acid additions were recorded. Additional copper was added and the process repeated until the free copper concentration was greater than 1×10^{-4} M.

Results

Potentiometric Titrations. Figure 1 shows the results of potentiometric titrations conducted at ionic strengths ranging between 0.003 and 0.1 N. Except for the titration at 0.003 N, any apparent hysteresis was within experimental error. The surface charge versus pH relationships are typical for oxides. For a given pH, the absolute value of the surface charge increases as ionic strength increases. Additionally, the pH where surface charge is zero (pH_{pzc}) is, within experimental precision, the same for all ionic strengths (*4, 13*). Here the pH_{pzc} is 8.9.

The pH_{pzc} determined here is at the high end of the range (~7.5−9.5) noted by other researchers. High pH_{pzc}s have been observed recently by more researchers who have taken care to exclude or minimize goethite exposure to CO_2 (*13, 22, 23, 29−31*). Theoretical analyses suggest that goethite pH_{pzc}s should be in the range of 9−10 (*22, 23, 32*). Carbonate can sorb to goethite (*33*); such sorption may affect surface charge and lower the pH_{pzc}.

At a given ΔpH from the pH_{pzc}, the surface charge density for this goethite is up to 50% higher than those of goethites studied by Hayes (*34*) and Lumsdon et al. (*30*). It is also higher than that observed by Hiemstra et al. (*22*) for high-surface area goethites but lower than what they observed for a 31 $m^2\ g^{-1}$ goethite (Supporting Information; *24*). Hiemstra et al. (*22*) suggest that rapid base addition during goethite synthesis (as done here) results in lower surface areas and higher surface charge densities.

Copper Binding. pH-statted copper titrations were conducted at ionic strengths of 0.01 and 0.1 N (Figure 2). Equilibrium constants for $Cu(OH)_x$ solution species and precipitates (*35*) indicate that concentrations of these species are negligible for the combinations of pH, pCu, and ionic strength encountered here. Our analyses consider only Cu^{2+}(aq) and sorbed copper species.

Goethite crystallographic analysis indicates that surface hydroxyl densities range from ~6 to 20 nm^{-2}, though not all sites are necessarily proton or metal reactive (*13, 22, 23, 36*). For this goethite, a reactive site density between 2 and 20 nm^{-2} corresponds to between 1.6×10^{-4} ($10^{-3.8}$) and 1.6×10^{-3} ($10^{-2.8}$) mol of sites per gram of goethite. The maximum observed copper surface loading, $\sim 2.5 \times 10^{-4}$ mol/g, then represents between 15 and 150% of the total reactive sites.

The pH 5 and 6 partitioning isotherms show a strong pH dependence [1.8−1.9 $(\Delta pCu/\Delta pH)_{Cu\ sorbed,\ I}$] but no obvious ionic strength dependence. This dependence is consistent with other oxide−divalent cation systems that show pH dependencies between 1 and 2 (Supporting Information; *24*). Isotherms show three ranges (Figure 3). Below $\sim 10^{-5}$ mol of copper bound/g (~1−7% of the total sites, Lo), data can be well fit by straight lines with slopes (log Cu bound/log-{Cu}) that range from 0.64 to 0.67. Between $\sim 10^{-5}$ and $\sim 10^{-4.3}$ mol of copper bound/g (3−30% of the total sites), curve slopes are 0.9−1.0 (Mid). Above this, the curve slopes drop to <0.5 (Hi). Slopes of <1 at surface loadings far from saturation are inconsistent with a single affinity site surface. Similar behavior has been noted in other cation−mineral systems (Supporting Information; *24*).

Inherent uncertainty in ISE measurements makes the uncertainty in calculated sorption at pH 4 significantly greater than that at pH 5 or 6. At pH 4, calculated copper sorption ranges from 20 (pCu 4) to 60% (pCu 6.5) of added copper. At pH 5 and 6, from 75 to >99.99% of added copper sorbs. If ISE measurements overestimate the pCu by 0.05 unit, the calculated surface loading is overestimated by 0.02, 0.04, and 0.3 log unit, respectively, for estimated 75, 60, and 20% sorption.

Proton Release. Figure 3 summarizes $Cu^{2+}-H^+$ exchange data. The figure shows incremental proton release, with *X* and *Y* axes calculated as follows:

TABLE 1. Goethite−Me^{2+} Surface Complexation Model Reactions[a]

surface species	mass action relation	equilibrium constant[b]
(1) SOH	SOH	−
(2) SOH_2^+	$SOH + H^+ \leftrightarrow SOH_2^+$	K_{a1}
(3) SO^-	$SOH \leftrightarrow SO^- + H^+$	K_{a2}
(4) $SOMe^+$	$SOH + Me^{2+} \leftrightarrow SOMe^+$	K_{Me}
(5) SOMeOH	$SOH + Me^{2+} + H_2O \leftrightarrow SOMeOH + 2H^+$	K_{MeOH}
(6) $(SO)_2Me$	$2SOH + Me^{2+} \leftrightarrow (SO)_2Me + 2H^+$	K_{biMe}
(7) $SO^-{-}Me^{2+}$	$SOH + Me^{2+} \leftrightarrow SO\text{-}\cdot\cdot Me^{2+} + H^+$	K_{S-Me}
(8) $SO^-{-}MeOH$	$SOH + Me^{2+} + H_2O \leftrightarrow SO^-{-}MeOH^+ + 2H^+$	K_{S^-MeOH}
(9) $SO^-{-}M^+$	$SOH + M^+ \leftrightarrow SO^- - M^+ + H^+$	K_{cat}
(10) $SOH_2^+{-}X^-$	$SOH + X^- + H^+ \leftrightarrow SOH_2{+}{-}X^-$	K_{an}
(11) $SOMe^+{-}X^-$	$SOH + Me^{2+} + X^- \leftrightarrow SOMe^+{-}X^-$	K_{Me-X}
(12) $-M^+$	$M^+ \leftrightarrow -M^+$	K_{cat*}
(13) $-X^-$	$X^- \leftrightarrow -X^-$	K_{an*}

$$K_{a1} = \frac{[SOH_2^+]f(-\psi_0)}{[SOH][H^+]} \qquad K_{a2} = \frac{[SO^-][H^+]f(\psi_0)}{[SOH]}$$

$$K_{Me} = \frac{[SOMe^+][H^+]}{[SOH][Me^{2+}]} \qquad K_{MeOH} = \frac{[SOMeOH][H^+]^2}{[SOH][Me^{2+}]}$$

$$K_{biMe} = \frac{[(SO)_2Me][H^+]^2}{[SOH]^2[Me^{2+}]} \qquad K_{S\cdot\cdot Me} = \frac{[SO^-\cdot\cdot Me^{2+}][H^+]f(\psi_0 - 2\psi_\beta)}{[SOH][Me^{2+}]}$$

$$K_{S\cdot\cdot MeOH} = \frac{[SO^-\cdot\cdot MeOH^+][H^+]^2 f(\psi_0 - \psi_\beta)}{[SOH][Me^{2+}]} \qquad K_{cat} = \frac{[SO^-\cdot\cdot M^+][H^+]}{[SOH][M^+]}$$

$$K_{an} = \frac{[SOH_2^+\cdot\cdot X^-]f(\psi_\beta - \psi_0)}{[SOH][H^+][X^-]} \qquad K_{Me\cdot\cdot X} = \frac{[SOMe^+\cdot\cdot X^-][H^+]f(\psi_\beta - \psi_0)}{[SOH][Me^{2+}][X^-]}$$

$$K_{cat*} = \frac{[\cdot\cdot M^+]f(\psi_\beta)}{[M^+]} \qquad K_{an*} = \frac{[\cdot\cdot X^-]f(-\psi_\beta)}{[X^-]} \qquad f(y) = \exp\left(\frac{-Fy}{RT}\right)$$

[a] Components: H^+, SOH (surface hydroxyl), Me^{2+} (specifically binding divalent metal cation), M^+ and X^- (indifferent electrolyte ions), and ψ (electrostatic potential in volts). [b] F = Faraday's constant (96 490 C mol^{-1}). R = gas constant (8.314 J mol^{-1} K^{-1}). T = absolute temperature, (kelvin). Brackets ([ ])denote concentrations. Braces ({ }) denote activity (moles per liter). Note that equilibrium constants for species 6, 12, and 13 are oxide concentration-dependent (*24*, *39*). For the triple-layer and modified triple-layer models, the relationships between surface charge (σ, C m^{-2}) and potential (ψ, volts) are as follows. $\sigma_0 = (\psi_0 - \psi_\beta)/C_1$ (A1). $\sigma_d = G_1(I,T)\sinh[G_2(\psi_d,T)] = (\psi_d - \psi_\beta)/C_2$ (A2). $\sigma_d + \sigma_\beta = -\sigma_0$ (A3). C_1 and C_2 are capacitances. Equation A2 represents the Poisson−Boltzman charge vs potential relationship for a charged flat plate (*1*). Equation A3 is the charge neutrality requirement. In the diffuse layer model, bulk water is assumed to directly abut the surface; there is no β layer; there are no capacitances. Equation A2 defines the charge vs potential relationship, and $\sigma_d = -\sigma_0$.

TABLE 2. Acid−Base Fits Used in Copper Analyses

	DLM	DLM	TLM	Mod TL
pH_{pzc}	8.9	8.9	8.9	8.9
[SOH] (sites/nm^2)	2.31	7.00	8.38	8.16
[SOH], moles sites/g	1.88×10^{-4}	5.70×10^{-4}	6.82×10^{-4}	6.64×10^{-4}
log K_{a1}	7.719	6.907	7.90	7.15
log K_{a2}	−10.088	−10.799	−9.90	−10.65
log K_{an}			8.334	−2.589
log K_{cat}			−9.332	−2.477
C_1			1.2	1.6
C_2			0.2	0.2

$$X_i = \frac{Cu_{b_i} + Cu_{b_{i-1}}}{2} \tag{1a}$$

$$Y_i = \frac{B_i - B_{i-1}}{Cu_{b_i} - Cu_{b_{i-1}}} \tag{1b}$$

where Y represent the incremental protons released per copper bound, B represents the moles of base added, Cu_b represents the moles of copper bound, i represents the titration point, and X midpoint of the moles of copper bound. Calculated releases generally range between 1.6 and 1.95 protons per copper bound. The 5−10% variability between replicate experiments (Figure 3A) indicates that pH, ionic strength, and surface loading dependencies suggested by Figure 3B may not be significant. Experimental uncertainties are highest at low (small titrant additions) and high (decreased fraction of added copper partitioning to goethite) surface loadings (*24*). The observed proton release is, within experimental error, equal to the observed copper binding pH dependence of 1.8−1.9. This equivalence between pH dependence and proton release was predicted in the thermodynamic analysis of Perona and Leckie (*37*).

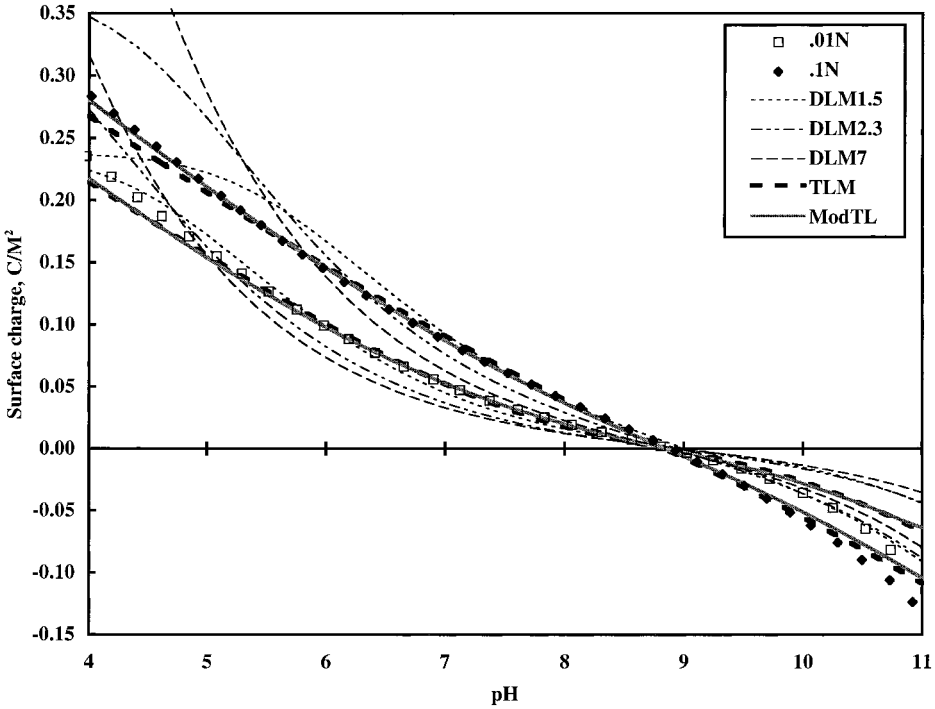

FIGURE 5. SCM fits of goethite acid−base data. Symbols are data, and lines are model fits. acid−base parameters are shown in Table 2.

TABLE 3. pH and Ionic Strength Dependencies of Divalent Cation SCM Complexes

		pCu for $10^{-6.5}$ moles Cu bound/per gram of goethite				$pCu_{0.01\,N} - pCu_{0.1\,N}$		$pCu_{pH\,6} - pCu_{pH\,5}$	
complex	log K[a]	pH 6, 0.01 N	pH 6, 0.1 N	pH 5, 0.01 N	pH 5, 0.1 N	pH 6	pH 5	0.01 N	0.1 N
				TLM					
$SOMe^+$	3.16	9.50	9.48	7.49	7.46	0.02	0.03	2.01	2.02
$SOMe^+(-X-)$[b]	2.93	9.50	9.62	7.59	7.70	−0.12	−0.11	1.91	1.92
SOMeOH	−5.72	9.50	9.48	7.48	7.46	0.02	0.02	2.02	2.02
$(SO)_2Me$[c]	−3.44	9.50	9.47	7.47	7.43	0.03	0.04	2.03	2.04
$SO^{--}Me^{2+}$	0.28	9.50	10.74	8.99	10.39	−1.24	−1.40	0.51	0.35
$SO^{--}MeOH^+$	−7.13	9.50	10.14	8.26	8.95	−0.64	−0.69	1.24	1.19
				Mod TL					
$SOMe^+$	2.44	9.50	9.66	7.68	7.82	−0.16	−0.13	1.82	1.85
SOMeOH	−5.78	9.50	9.48	7.48	7.46	0.02	0.02	2.02	2.02
$(SO)_2Me$[c]	−3.57	9.50	9.47	7.46	7.42	0.03	0.04	2.04	2.05
$SO^{--}Me^{2+}$	0.22	9.50	10.86	8.71	10.05	−1.36	−1.33	0.79	0.81
$SO^{--}MeOH^+$	−6.82	9.50	10.16	8.07	8.65	−0.66	−0.58	1.43	1.51
				DLM with 2.3 Sites/nm²					
$SOMe^+$	3.08	9.50	9.76	7.78	7.99	−0.26	−0.21	1.72	1.77
SOMeOH	−5.15	9.50	9.38	7.37	7.07	0.12	0.30	2.13	2.31
$(SO)_2Me$[c]	−2.31	9.50	9.26	7.23	6.64	0.24	0.59	2.27	2.62
				DLM with 7.0 Sites/nm²					
$SOMe^+$	2.35	9.50	9.80	7.82	8.11	−0.30	−0.29	1.68	1.69
SOMeOH	−5.73	9.50	9.47	7.47	7.40	0.03	0.07	2.03	2.07
$(SO)_2Me$[c]	−3.45	9.50	9.44	7.44	7.30	0.06	0.13	2.06	2.14

[a] Constant necessary to bind $10^{-6.5}$ mol of Cu/g of goethite for pCu 9.5, pH 6.0, and $I = 0.01$ N. [b] Consists of $SOMe^+$ and $SOMe^+-X^-$ complexes; $K_{SOMe^+-X^-} = 10^{0.434}K_{SOMe^+}$. [c] Equilibrium constant proportional to 1/[goethite] (liters per gram) (*24*, *39*). See Table 2 for acid/base parameters.

Modeling

We have modeled the potentiometric and copper titration data with the Diffuse layer model [DLM (*38*)], the triple-layer model [TLM (*18, 19*)], and a modified triple-layer model [Mod TL (*24, 39*)]. We assume a single, planar surface and amphoteric surface sites which can be in one of three protonation states (Figure 4 and Table 1). The DLM assumes a surface immersed in a point charge-containing, constant dielectric medium, with a diffuse layer that directly abuts the surface. Any net charge on the oxide surface is exactly compensated by a net charge, of opposite sign, in the diffuse layer. Diffuse layer ions are distributed according to the Poisson−Boltzmann relation (*3, 5, 13*). Surface species 1−6 of Table 1 and Figure 4 represent DLM species.

The TLM interfacial region structure implicitly accounts for the finite size of ionic and molecular entities, and for surface−solvent interactions that may affect dielectric properties of the medium by dividing the region adjacent to the surface into planes. Ions that interact with the surface reside in the planes. Charge versus potential relationships are calculated by assuming the planes are parallel plates and the medium between them has a fixed capacitance. A diffuse

layer, exactly comparable to that of the DLM, begins a few molecular (ionic) diameters from the oxide surface. TLM surface species include species 1−11 of Table 1 and Figure 4.

The Mod TL is identical to the TLM except in the handling of indifferent electrolyte−surface interactions. In both models, electrolyte ions accumulate in the β-plane to screen oxide (0 plane) charge. The TLM assumes that β-plane electrolyte ions form complexes with oxide surface sites (species 9 and 10). In the Mod TL, these ions accumulate to screen surface charge, but do not form complexes with surface sites (species 12 and 13).

FITEQL v3.1 (*40*) was used to determine combinations of equilibrium constants and oxide site concentrations that fit potentiometric and pH-stated copper titration data. Combinations of surface site density, equilibria for surface species 2 and 3 (all models), 9 and 10 (TLM), and 12 and 13 (Mod TL), and capacitances C_1 and C_2 (TLM and Mod TL) were determined by fitting the potentiometric titration data. These acid−base values were used in fits of metal species (surface species 4−8 and 11) to the copper binding data.

Modeling Potentiometric Titration Results. Data at pHs <10 from acid (second) legs of titrations at 0.01, 0.03, and 0.1 N ionic strength, were used for fitting. DLM fits require a surface site density and two acidity constants; all parameters can be fit simultaneously. The TLM and Mod TL have seven fitting parameters: site density, four equilibrium constants, and two capacitances. Typically, many combinations of these parameters can successfully replicate acid−base behavior (*41*). Attempts to simultaneously fit all parameters will not converge. We determined parameter combinations by fixing acid−base equilibria (surface species 2 and 3) and capacitances C_1 and C_2 and fitting for the site density and electrolyte binding constants: surface species 9 and 10 (TLM) or 12 and 13 (Mod TL). Acid/base equilibria and capacitances were varied parametrically (*41*). Robertson and Leckie (*39*) include a detailed description of the procedure and the results. Table 2 lists the acid−base parameter combinations used in the copper-modeling fits. Figure 5 shows how these fits replicate the acid−base data. The TLM and Mod TL fits are quite good; the DLM replicates the data poorly. The 2.3 and 7.0 sites nm^{-2} fits were obtained by fixing the site density and fitting the acidity constants. These site densities have been suggested [2.3 (*13*)] or used [7.0 (*34*)] by others. They were employed because the fitted DLM site density (1.5 nm^{-2}) was significantly lower than the maximum observed partitioning of copper to the goethite surface (~3 nm^{-2}).

Modeling Goethite−Copper Binding. A number of possible surface complexes (complexes 4−8 and 11) were considered in the attempt to replicate the observed copper partitioning. For metal surface loadings far from saturation, the pH and ionic strength dependencies of model complexes can be calculated using the equilibrium relations of Table 1 and values for [SOH], ψ_0, and ψ_β determined from copper-free simulations (*39*). The procedure first requires determination of an equilibrium constant for a complex for a given surface loading, pMe, pH, and ionic strength. Using the calculated equilibrium constant for a complex, pMes for other pH and ionic strength combinations can be determined. Table 3 summarizes the results of such an analysis.

The experimental data show little, if any, ionic strength dependence, and the pH dependence, $(\Delta pCu/\Delta pH)_{Cu\ sorbed,\ I}$, is 1.8−1.9. Table 3 shows that TLM and Mod TL outer sphere complexes (SO^--Me^{2+} and SO^--MeOH^+) have ionic strength dependencies that are much higher and pH dependencies that are much lower than those observed. The calculated dependencies for TLM and Mod TL inner sphere complexes are much closer to those observed. Of the DLM complexes considered, the SOMeOH, 7 sites/nm^2 fit appears to be the best match.

The TLM $SOMe^+(-X^-)$ fit represents a system where both $SOMe^+$ and $SOMe^+-X^-$ complexes are formed (analogous to the $SOH_2^+/SOH_2^+-X^-$ couple). For this couple, many log K combinations could fit a particular combination of pH, pCu, I, and copper bound. We chose a combination where the propensity of the electrolyte anion (X^-) to associate with an $SOMe^+$ species is identical to its propensity to associate with an SOH_2^+ species.

$$\log K_{Me-X} = \log K_{Me} + \log K_{an} - \log K_{a1} = \log K_{Me} + C \quad (2)$$

DLM, TLM, and Mod TL complexes were fit to regressions of the pH 5 and 6 data (0.01 and 0.1 N). Regressions were used because the total number of data points (207) was too great for FITEQL v3.1 to handle. Fit highlights are summarized in Table 4 and Figure 6. More extensive summaries are available (Supporting Information; *24*). Fit quality is indicated by FITEQL's goodness of fit term, WSOS/DF; the lower the value, the better the fit (*40*).

Fits employing a single class of copper binding sites yielded poor results in all cases, primarily because fitted log Cu bound versus log{Cu} slopes (~1, see Figure 7) in the region from $10^{-6.5}$ to $10^{-4.8}$ mol of Cu bound/g of goethite differ substantially from observed values (~0.65). Addition of a second class of copper sites (high-affinity, low-concentration) generally improved fits substantially. This second site class typically represented ~0.2−0.5% of the total site concentrations. Fitting site concentrations for both classes often resulted in total site concentrations that were substantially lower than the total site concentrations derived from acid/base fits. To maintain total site concentrations at the acid/base fit values (Table 2) a third, non-copper binding site class (20−60% of the total sites) was included, when necessary, in the fitting process. When this third site class was allowed to bind copper, goodness of fit values (WSOS/DF) improved substantially in some cases (TLM SOCuOH) and only slightly in others (TLM $SOCu^+$).

Fitting with two complexes ($SOCu^+$ and SOCuOH) had almost no effect on TLM fits but substantially improved fits for the Mod TL and DLM. Mod TL SOCuOH fits were essentially identical to comparable TLM fits, while the best two- and three-copper binding site DLM SOCuOH fits had WSOS/DF values of 43 and 18, respectively (Supporting Information).

Fits employing both SOCuOH and either $SOCu^+$ or the $SOCu^+(-ClO_4^-)$ couple did not converge if all equilibrium constants were fitted simultaneously. To achieve convergence, we fit $K_{_Me}$s for each site class. $K_{\_MeOH}$ was related to $K_{\_Me}$ through a single, fitted proportionality constant (K^*_{OH}).

$$K_{-MeOH} = K_{-Me}K_{OH}^* \quad (3)$$

Discussion

The experimental data suggest the presence of, and successful model replication require inclusion of, multiple classes of copper binding site classes. Generally, model fits improve significantly when a high-affinity copper site with a concentration of ~1 to 2×10^{-6} mol of sites/g of goethite (~0.01−0.02 site nm^{-2}) is included. Crystallographic analyses suggest that several types of surface hydroxyls exist on goethite crystal faces; however, densities are typically greater than 1 site nm^{-2} for a given class of sites on a particular crystal face (*15*, *22*, *23*, *42*, *43*). To represent an overall site density of 0.01 nm^{-2}, a particular site class would have to be present on a crystal face that accounts for <1% of total surface area. Thus, high-affinity sites may be located at edges, kinks, steps, or dislocations on the crystal surface.

Experimentally observed pH dependencies (1.8−1.9) and proton releases (1.65−1.95) are, within experimental error,

TABLE 4. SCM Copper Binding Fits[a]

	$SOCu^+$					SOCuOH	
	TLM	TLM (Figure 6a)	TLM	Mod TL (Figure 6b)	DLM, 7 (Figure 6c)	TLM (Figure 6e)	TLM (Figure 6g)[e]
[S1OH][b]	**6.81×10^{-4}**	5.26×10^{-4}	**4.80×10^{-4}**	**6.64×10^{-4}**	**5.70×10^{-4}**	2.05×10^{-4}	**5.50×10^{-4}**
[S2OH][c]		1.07×10^{-6}	**2.00×10^{-4}**	5.28×10^{-7}	9.66×10^{-7}	2.05×10^{-6}	**1.30×10^{-4}**
[S3OH]		**1.50×10^{-4}**	1.00×10^{-6}			**4.80×10^{-4}**	1.20×10^{-6}
log K_1	2.586	2.544	2.066	1.707	1.390	−6.100	−8.153
log K_2[d]		5.968	2.831	5.490	4.859	−3.289	−5.776
log K_3			6.000				−2.978
WSOS/DF	83.0	17.3	16.9	50.0	111.8	37.7	12.7

	$SOCu^+(\cdot\cdot ClO_4^-)$			
	TLM	TLM	TLM (Figure 6d)	TLM (Figure 6f)[e]
[S1OH]	**6.81×10^{-4}**	**6.81×10^{-4}**	2.78×10^{-4}	**5.60×10^{-4}**
[S2OH]		2.27×10^{-6}	1.36×10^{-6}	**1.20×10^{-4}**
[S3OH]			**4.00×10^{-4}**	1.06×10^{-6}
log K_{1Me}	2.118	1.887	2.396	1.318
log K_{2Me}		5.159	5.452	2.755
log K_{3Me}				5.596
log $K_{1Me\cdots X}$	2.552	2.321	2.830	1.752
log $K_{2Me\cdots X}$		5.593	5.886	3.189
log $K_{3Me\cdot b,\cdot X}$				6.030
WSOS/DF	136.9	22.3	14.5	11.0

	$SOCu^+$ and SOCuOH					
	TLM	TLM	Mod TL	Mod TL (Figure 6i)[e]	DLM, 7	DLM, 7 (Figure 6j)[e]
[S1OH]	**4.00×10^{-4}**	**5.50×10^{-4}**	**2.73×10^{-4}**	**5.20×10^{-4}**	2.16×10^{-4}	**4.40×10^{-4}**
[S2OH]	1.04×10^{-6}	**1.3×10^{-4}**	1.06×10^{-6}	**1.40×10^{-4}**	1.88×10^{-6}	**1.30×10^{-4}**
[S3OH]	**2.80×10^{-4}**	1.120×10^{-6}	**4.00×10^{-4}**	1.13×10^{-6}	**3.50×10^{-4}**	1.18×10^{-6}
log K_{1Me}	2.667	−0.669	1.900	−0.239	1.319	−0.634
log K_{2Me}	5.981	1.706	5.020	1.948	4.161	1.515
log K_{3Me}		4.505		4.781		4.304
log K_{1MeOH}	−8.343	−8.169	−7.168	−8.429	−6.494	−8.218
log K_{2MeOH}	−5.029	−5.794	−4.048	−6.242	−3.652	−6.069
log K_{3MeOH}		−2.995		−3.409		−3.280
WSOS/DF	16.7	12.7	15.1	6.8	26.1	6.2

[a] Within a model fit acid base properties for all site classes are identical (Table 2). [b] Site concentration (moles per gram of goethite); bold values were fixed, not fit. [c] If blank there are no sites in this class. [d] If blank, site class does not bind copper. [e] Figures included with Supporting Information.

equal. This correspondence was predicted, on thermodynamic grounds, by Perona and Leckie (*37*). This correspondence also occurs in FITEQL SCM simulations (data not shown).

The copper fits (Table 4, Figure 6, and the Supporting Information**)** indicate that the low surface loading analysis (Table 3) is useful for initial screening of potential surface complexes. However, factors not considered in the low loading analysis also affect the ability of a complex to fit a data set. Table 3 suggests that TLM $SOMe^+$ and both TLM and Mod TL SOMeOH and $(SO)_2Me$ complexes behave virtually identically. The SOCuOH and $(SO)_2Cu$ fits do behave virtually identically, though the $(SO)_2Cu$ fits require a higher site concentration for some site classes (*24*; Supporting Information). On the other hand, two-copper site TLM $SOCu^+$ fits match the data better than two-site SOCuOH or $(SO)_2Cu$ fits, while the situation is reversed for three-copper site fits. Figures 7 and 8 suggest why. Figure 7's constant pH, single-site, partitioning isotherms include "Langmuir" fits that represent metal complexation to a simple ligand, L (no protonation or electrostatic considerations). SOMeOH and $(SO)_2Me$ isotherms show little deviation from Langmuir curves because their formation does not depend on surface potentials (ψ_s, Table 1). Where surface potentials influence partitioning, isotherm curvature depends on the model employed and the nature of the complex (*24, 39*). For a single class of binding sites, TLM $SOMe^+$ and $SOMe^+(-X^-)$ complexes match the experimentally observed, high-surface loading, curvature well. For SOMeOH and $(SO)_2Me$ complexes, inclusion of a second, high-concentration site class improves the correspondence between the overall isotherm and observed curvature (Figure 8).

For this TLM fit, complexes influenced by electrostatics will not saturate the available surface sites ($10^{-3.167}$ M). Mod TL behavior is qualitatively similar to that of the TLM, while all DLM complexes can saturate available sites (*24, 39*; Supporting Information).

At low surface loadings, the TLM $SOMe^+(-X^-)$ couple and the Mod TL $SOMe^+$ complex match the observed Cu partitioning pH dependence equally well (Table 3). However, the TLM couple does a better job of replicating the data. The lower ionic strength dependency of the TLM couple is part of the reason. Additionally, at high surface loadings, the Mod TL $SOMe^+$ complex's pH and ionic strength dependencies change in ways that do not match the data (data not shown).

Summary

Copper partitioning to goethite is strongly pH-dependent, but is affected only minimally by changes in ionic strength. The copper binding observed is inconsistent with a single-plane, single-site class system. Partitioning can be replicated well by assuming existence of a second high-affinity copper binding site, with a site density of ~0.01−0.02 nm^{-2}. This low density suggests sites located at steps, kinks, etc., on the

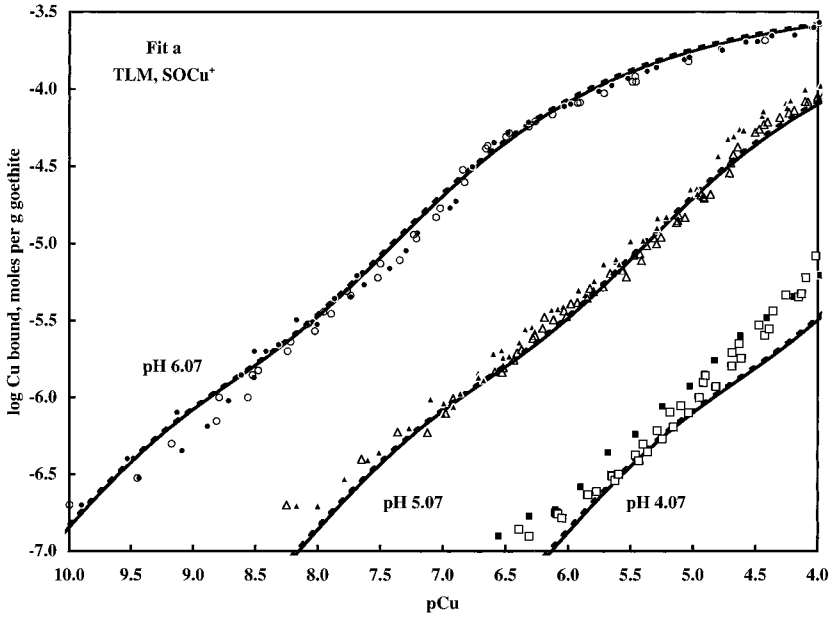
Fit a
TLM, SOCu+
pH 6.07
pH 5.07
pH 4.07
log Cu bound, moles per g goethite
pCu
-3.5
-4.0
-4.5
-5.0
-5.5
-6.0
-6.5
-7.0
10.0
9.5
9.0
8.5
8.0
7.5
7.0
6.5
6.0
5.5
5.0
4.5
4.0

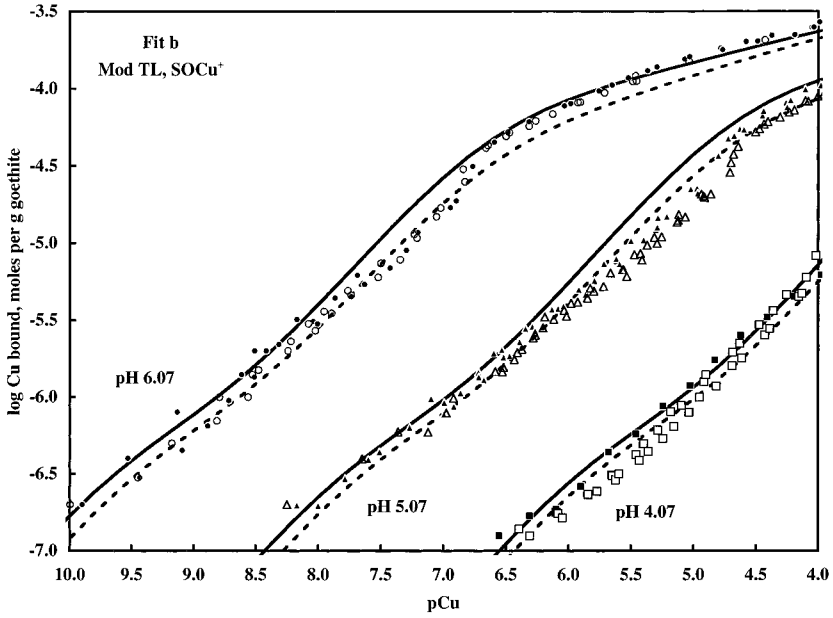
Fit b
Mod TL, SOCu+
pH 6.07
pH 5.07
pH 4.07
log Cu bound, moles per g goethite
pCu
-3.5
-4.0
-4.5
-5.0
-5.5
-6.0
-6.5
-7.0
10.0
9.5
9.0
8.5
8.0
7.5
7.0
6.5
6.0
5.5
5.0
4.5
4.0

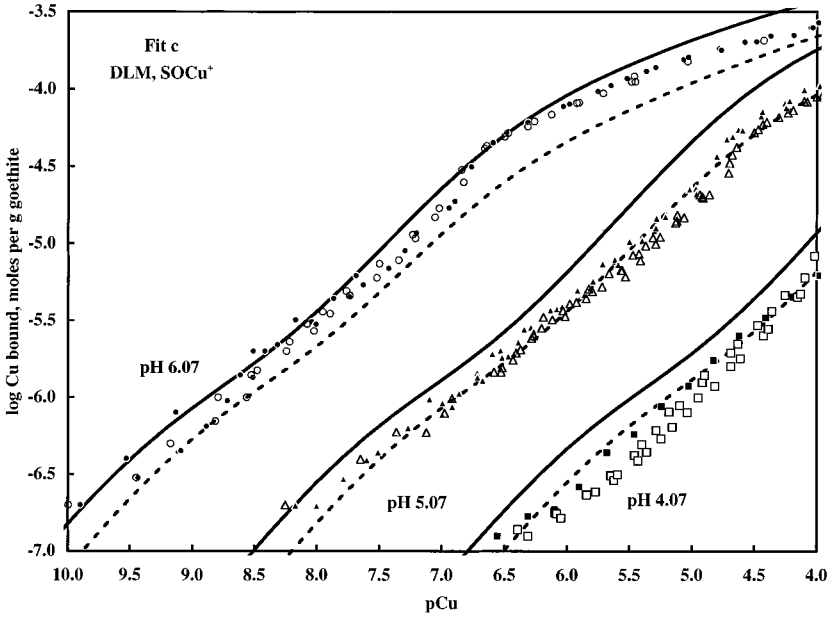
Fit c
DLM, SOCu+
pH 6.07
pH 5.07
pH 4.07
log Cu bound, moles per g goethite
pCu
-3.5
-4.0
-4.5
-5.0
-5.5
-6.0
-6.5
-7.0
10.0
9.5
9.0
8.5
8.0
7.5
7.0
6.5
6.0
5.5
5.0
4.5
4.0

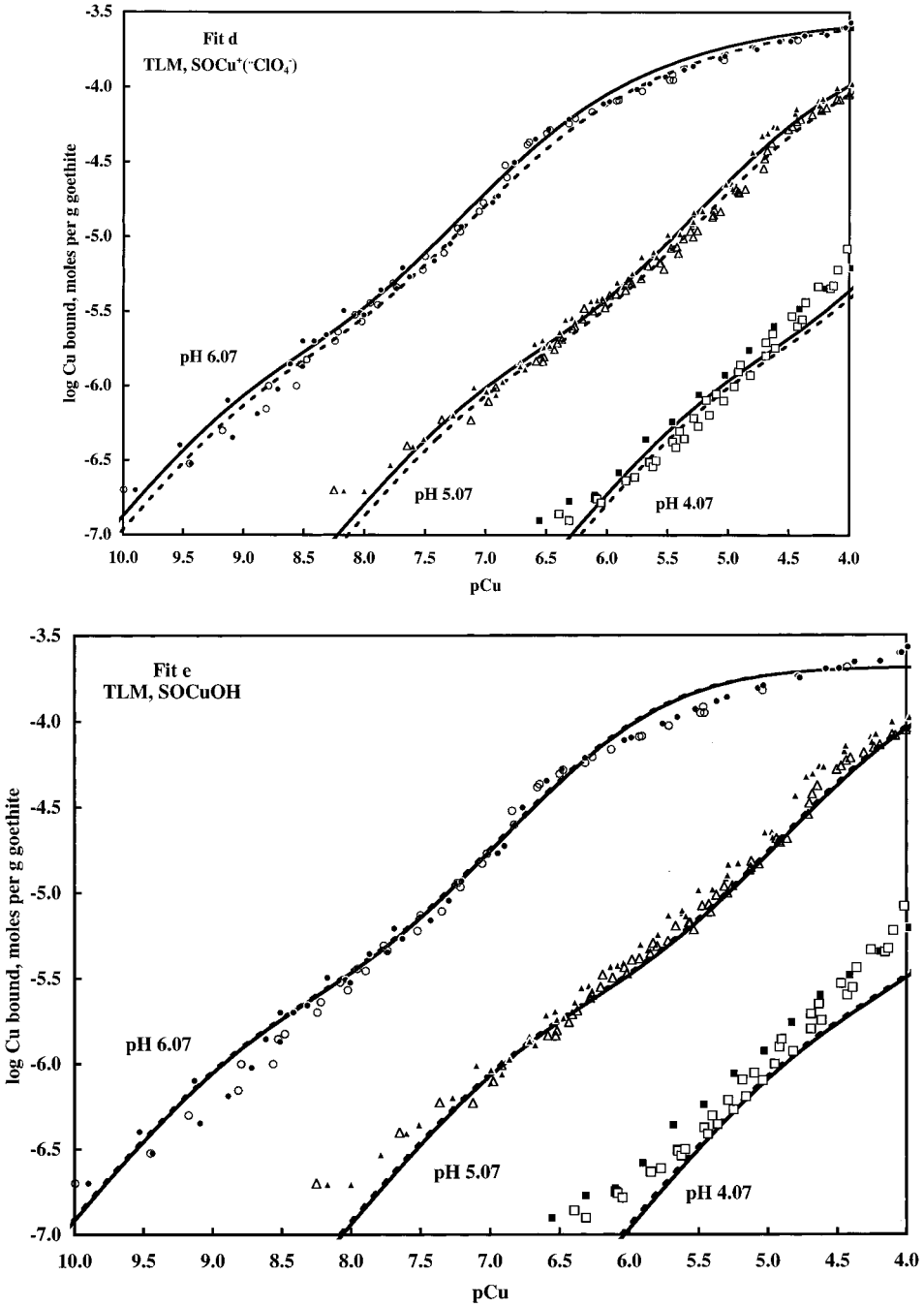

FIGURE 6. Selected SCM fits to copper binding data. Refer to Table 4 for a fit's site concentrations and equilibrium constants. Symbols represent data points (0.1 N, solid; and 0.01 N, open); lines are model fits (0.1 N, solid; and 0.01 N, dashed).

mineral surface. A separate, high-affinity crystal face representing a small fraction of total surface area might also be able to account for the observations.

Three surface complexation models (DLM, TLM, and Mod TL), differing in their representation of the region directly adjacent to the oxide surface, were used to replicate and analyze the experimental observations. Unlike the TLM and Mod TL, the DLM is unable to reasonably replicate the goethite's acid−base properties. However, all three models can successfully replicate observed copper partitioning over a 1000-fold range in surface loadings (2×10^{-7} to 2×10^{-4} mol of copper/g of goethite; 4×10^{-9} to 4×10^{-6} mol m^{-2}) for two pHs and two ionic strengths.

The $SOMe^{+}(-X^{-})$ or the comparable $SL^{-}(-M^{+})$ couple is not typically employed in TLM analyses. Their consideration derives logically from the model structure which uses SOH_2^{+}-$(-X^{-})$ and $SO^{-}(-M^{+})$ couples. The couple has properties that differ from those of other TLM complexes and was able to fit the data well.

A rose may be a rose may be a rose, but SCM complexes are not roses. The pH and ionic strength dependencies for a particular complex ($SOMe^{+}$, for instance) can vary significantly between models, and even between model fits (DLM). Venema et al. (*15*) also found that the properties of an $SOMe^{+}$ complex depended upon the SCM employed, while Katz and Hayes (*44*) saw that response depended on the TLM fit used. Though SCM equilibrium constants of the form used here (Table 2) are called "intrinsic", they are intrinsic only in the sense that they are designed to be independent of ionic strength. These constants are part of an indivisible package; this package includes the model structure and calculated site concentrations, capacitances,

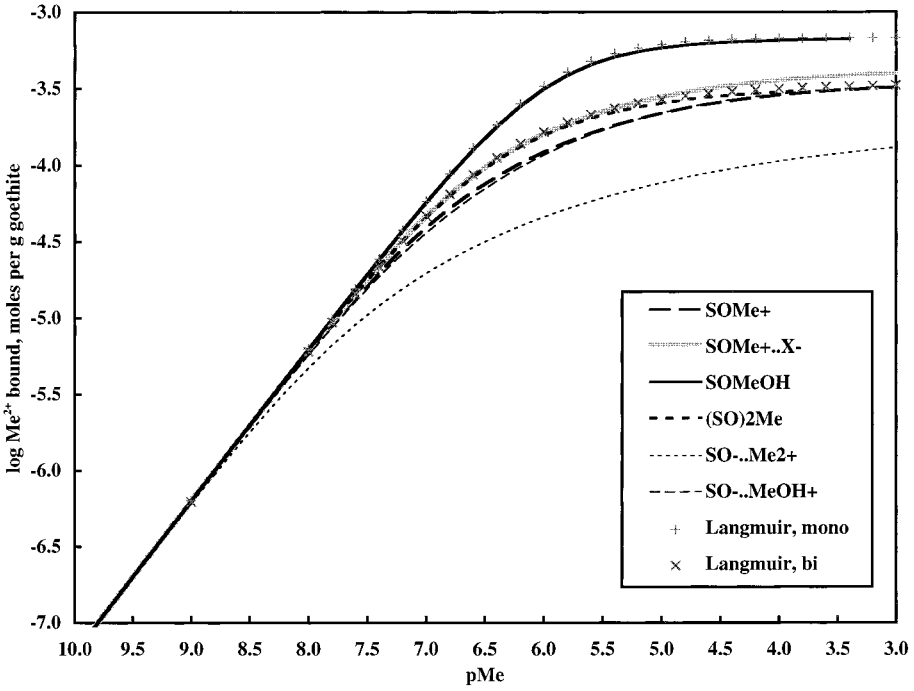

FIGURE 7. TLM surface loading vs pMe for various surface species. Single Me^{2+} affinity site; 6.8×10^{-4} ($10^{-3.17}$) mol of sites/g of goethite. DLM and Mod TL properties are similar (*24, 39*; Supporting Information).

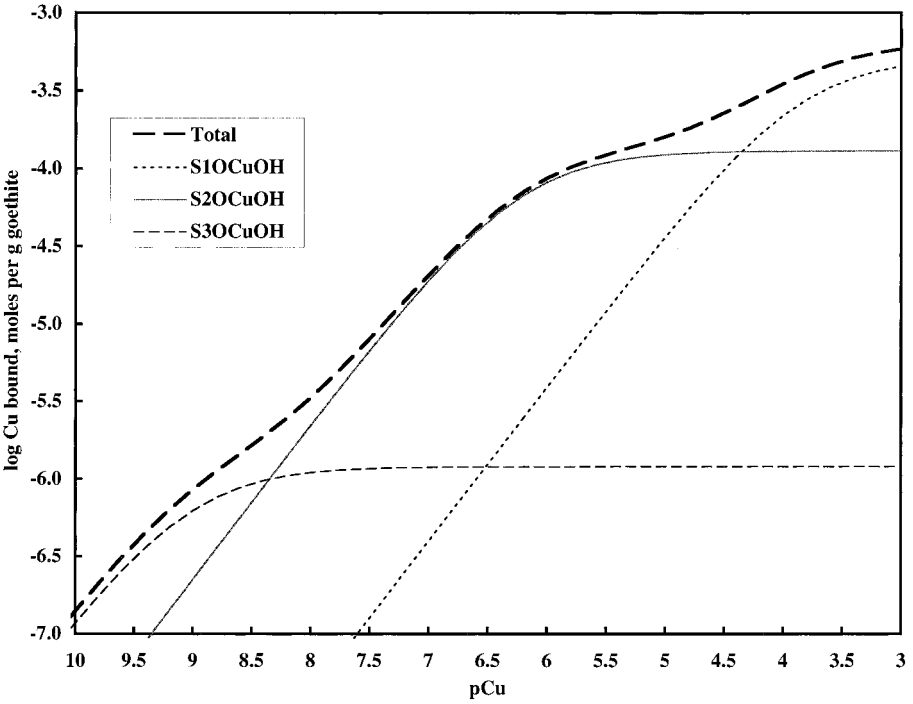

FIGURE 8. Overall and individual site surface loadings vs pCu for the three-binding site TLM SOCuOH complex.

and acid−base, electrolyte, and metal binding constants. Small differences in the assumed structure of the interfacial region can strongly affect model behavior; of particular importance are the effects of pH and ionic strength on [SOH] and electrostatic potentials (ψ_) (*39*; Supporting Information).

Considerable spectroscopic evidence suggests that surface precipitates or polymers can develop on oxide surfaces at moderate to high surface loadings (*45*−*49*). Though the behavior observed here can be replicated without invoking precipitation or polymerization reactions, this does not preclude their existence. Simulations incorporating such behavior may also be able to mimic the observed partitioning (*50, 51*).

Our copper partitioning data did not provide information sufficient to select a clearly "best" model or surface complex. Experimental data covering additional pHs or ionic strengths might have further limited acceptable fits. More importantly, a better understanding of the nature and concentration of surface sites and the properties of the interfacial region must be coupled with direct evidence of surface complex structure if we are to be confident that the models are more than just replicative tools.

Acknowledgments

This work was funded, in part by Electric Power Research Institute Grant RP-2485-13. We thank four anonymous

reviewers who put considerable time, effort, and intelligence into their critiques of the original manuscript. We believe that the paper is substantially improved because of their efforts.

Supporting Information Available

Metal binding properties of polyligands and SCM copper binding fits (2 tables and 4 figures) (17 pages). Ordering information is given on any current masthead page.

Literature Cited

(1) Nriagu, J. O. *Nature* **1989**, *338*, 47.
(2) Nriagu, J. O.; Pacyna, J. M. *Nature* **1988**, *333*, 134.
(3) Morel, F. M. M.; Hering, J. G. *Principles and Applications of Aquatic Chemistry*; Wiley-Interscience: New York, 1993; 588 p.
(4) Stumm, W.; Morgan, J. *Aquatic Chemistry*, 3nd ed.; John Wiley & Sons: New York, 1996; 1022 p.
(5) Sposito, G. *The Surface Chemistry of Soils*; Oxford University Press: New York, 1984; 234 p.
(6) Dixon, J. B.; Weed, S. B. *Minerals in Soil Environment*; Soil Science Society of America: Madison, WI, 1989; 1244 p.
(7) Robertson, A. P.; Leckie, J. O. *Environ. Sci. Technol.*, submitted for publication, 1998.
(8) Robertson, A. P.; Leckie, J. O. *Environ. Sci. Technol.*, submitted for publication, 1998.
(9) Keil, R. G.; Tsamakis, E.; Fuh, C. B.; Giddings, J. C.; Hedtes, J. I. *Geochim. Cosmochim. Acta* **1994**, *58*, 879.
(10) Davis, J. A.; Gloor, R. *Environ. Sci. Technol.* **1981**, *15*, 1223.
(11) Loder, T. C.; Liss, P. S. *Limnol. Oceanogr.* **1985**, *30*, 418.
(12) Tipping, E. *Mar. Chem.* **1986**, *18*, 161.
(13) Davis, J. A.; Kent, D. B. In *Mineral-Water Interface Geochemistry*; Hochella, M. F. J., White, A. F., Eds.; Mineralogical Society of America: Washington, DC, 1990; Vol. 23, pp 177−260.
(14) Stumm, W. *Aquatic Surface Chemistry: Chemical Processes at the Particle−Water Interface*; John Wiley & Sons: New York, 1987; 520 p.
(15) Venema, P.; Hiemstra, T.; van Riemsdijk, W. H. *J. Colloid Interface Sci.* **1996**, *181*, 45.
(16) Westall, J.; Hohl, H. *Adv. Colloid Interface Sci.* **1980**, *12*, 265.
(17) Schindler, P. W.; Stumm, W. In *Aquatic Surface Chemistry*; Stumm, W., Ed.; Wiley-Interscience: New York, 1987; pp 83−110.
(18) Hayes, K. F.; Leckie, J. O. *J. Colloid Interface Sci.* **1987**, *115*, 564.
(19) Hayes, K. F.; Papelis, C.; Leckie, J. O. *J. Colloid Interface Sci.* **1988**, *125*, 717.
(20) Charmas, R.; Piasecki, W.; Rudzinski, W. *Langmuir* **1995**, *11*, 3199.
(21) Barrow, N. J.; Bowden, J. W.; Posner, A. M.; Quirk, J. P. *Aust. J. Soil Res.* **1981**, *19*, 309.
(22) Hiemstra, T.; de Wit, J. C. M.; van Riemsdijk, W. H. *J. Colloid Interface Sci.* **1989**, *133*, 105.
(23) Hiemstra, T.; van Riemsdijk, W. H.; Bolt, G. H. *J. Colloid Interface Sci.* **1989**, *133*, 91.
(24) Robertson, A. P. Ph.D. Thesis, Stanford, Stanford, CA, 1996.
(25) Atkinson, R. J.; Posner, A. M.; Quirk, J. P. *J. Phys. Chem.* **1967**, *71*, 550.
(26) *Standard Methods for the Examination of Water and Wastewater*; American Public Health Association: Washington, DC; 1992.
(27) Altmann, R. S. Ph.D. Thesis, Stanford, Stanford, CA, 1984.
(28) Benedetti, M. F.; Milne, C. J.; Kinniburgh, D. G.; van Riemsdijk, W. H.; Koopal, L. *Environ. Sci. Technol.* **1995**, *29*, 446.
(29) James, R. O.; Parks, G. A. *Surf. Colloid Sci.* **1982**, *12*, 119.
(30) Lumsdon, D. G.; Evans, L. J. *J. Colloid Interface Sci.* **1994**, *164*, 119.
(31) Zeltner, W. A.; Anderson, M. A. *Langmuir* **1988**, *4*, 469.
(32) Sverjensky, D. A. *Geochim. Cosmochim. Acta* **1994**, *58*, 3123.
(33) van Geen, A.; Robertson, A. P.; Leckie, J. O. *Geochim. Cosmochim. Acta* **1994**, *58*, 2073.
(34) Hayes, K. F. Ph.D. Thesis, Stanford, Stanford, CA, 1987.
(35) Lindsay, W. L. *Chemical Equilibria in Soils*; Wiley-Interscience: New York, 1979; 347 p.
(36) Hiemstra, T.; van Riemsdijk, W. H. *J. Colloid Interface Sci.* **1996**, *179*, 488.
(37) Perona, M. J.; Leckie, J. O. *J. Colloid Interface Sci.* **1985**, *106*, 64.
(38) Dzombak, D.; Morel, F. M. M. *Surface Complexation Modeling Hydrous Ferric Oxide*; John Wiley & Sons: New York, 1990; 393 p.
(39) Robertson, A. P.; Leckie, J. O. *J. Colloid Interface Sci.* **1997**, *188*, 444.
(40) Herbelin, A.; Westall, J. *FITEQL, Version 3.1*; Department of Chemistry, Oregon State University: Corvallis, OR, 1994; Report 94-01.
(41) Hayes, K. F.; Redden, G.; Ela, W.; Leckie, J. O. *J. Colloid Interface Sci.* **1991**, *142*, 448.
(42) Hiemstra, T.; van Riemsdijk, W. H. *Colloids Surf.* **1991**, *59*, 7.
(43) Venema, P.; Hiemstra, T.; van Riemsdijk, W. H. *J. Colloid Interface Sci.* **1996**, *183*, 515.
(44) Katz, L. E.; Hayes, K. F. *J. Colloid Interface Sci.* **1995**, *170*, 477.
(45) Towle, S. N.; Bargar, J. R.; Brown, G. E., Jr.; Parks, G. A. *J. Colloid Interface Sci.* **1997**, *187*, 62.
(46) Bargar, J. R.; Brown, G. E., Jr.; Parks, G. A. *Geochim. Cosmochim. Acta* **1997**, *61*, 2617.
(47) Charlet, L.; Manceau, A. A. *J. Colloid Interface Sci.* **1992**, *148*, 443.
(48) Chisholm-Brause, C.; Hayes, K. F.; Roe, A. L.; Brown, G. E., Jr.; Parks, G. A.; Leckie, J. O. *Geochim. Cosmochim. Acta* **1990**, *54*, 1897.
(49) Eggleston, C. M.; Stumm, W. *Geochim. Cosmochim. Acta* **1993**, *57*, 4843.
(50) Katz, L. E.; Hayes, K. F. *J. Colloid Interface Sci.* **1995**, *170*, 491−501.
(51) Farley, K. J.; Dzombak, D. A.; Morel, F. M. M. *J. Colloid Interface Sci.* **1985**, *106*, 226.
(52) Honeyman, B. D. Ph.D. Thesis, Stanford, Stanford, CA, 1984.
(53) Barrow, N. J.; Gerth, J.; Brummer, G. W. *J. Soil Sci.* **1989**, *40*, 437.
(54) Dzombak, D. A.; Morel, F. M. M. *Environ. Prog.* **1987**, *6*, 133.
(55) Benjamin, M. M.; Leckie, J. O. *J. Colloid Interface Sci.* **1981**, *79*, 209.
(56) Quigley, M. S.; Honeyman, B. D.; Santschi, P. H. *Aquat. Geochem.* **1996**, *1*, 277.
(57) Cabaniss, S. E.; Shuman, M. S. *Geochim. Cosmochim. Acta* **1988**, *52*, 185.

Received for review November 11, 1997. Revised manuscript received May 12, 1998. Accepted May 26, 1998.

ES9709942